IOPscience iopscience.iop.org

Home Search Collections Journals About Contact us My IOPscience

Super-high density Si quantum dot thin film utilizing a gradient Si-rich oxide multilayer structure

This content has been downloaded from IOPscience. Please scroll down to see the full text.

2013 Nanotechnology 24 195701

(http://iopscience.iop.org/0957-4484/24/19/195701)

View the table of contents for this issue, or go to the journal homepage for more

Download details:

IP Address: 140.113.38.11
This content was downloaded on 25/04/2014 at 09:55

Please note that terms and conditions apply.

Nanotechnology **24** (2013) 195701 (7pp) doi:10.1088/0957-4484/24/19/195701

Super-high density Si quantum dot thin film utilizing a gradient Si-rich oxide multilayer structure

Kuang-Yang Kuo, Pin-Ruei Huang and Po-Tsung Lee

Department of Photonics and Institute of Electro-Optical Engineering, National Chiao Tung University, 1001 Ta-Hsueh Road, Hsinchu 30010, Taiwan

E-mail: potsung@mail.nctu.edu.tw

Received 16 January 2013, in final form 22 March 2013
Published 12 April 2013
Online at stacks.iop.org/Nano/24/195701

Abstract

A gradient Si-rich oxide multilayer (GSRO-ML) deposition structure is proposed to achieve super-high density Si quantum dot (QD) thin film formation while preserving QD size controllability for better photovoltaic properties. Our results indicate that the Si QD thin film using a GSRO-ML structure can efficiently increase the QD density and control the QD size. Its optical properties clearly promise the capability of effective bandgap engineering even though these QDs are closely formed. The Si QD thin film using a GSRO-ML structure obviously reveals better electro-optical properties than those using a [silicon dioxide/silicon-rich oxide] multilayer ([SiO_2/SRO]-ML) structure owing to the better optical absorption and carrier transport properties. Therefore, we successfully demonstrate that our proposed GSRO-ML structure has great potential for application in solar cells integrating Si QD thin films.

(Some figures may appear in colour only in the online journal)

1. Introduction

Recently, nano-crystalline silicon quantum dot (QD) thin films have been extensively studied due to their unique properties [1, 2] and applied to various optoelectronic devices such as solar cells (SCs) [3], light-emitting devices (LEDs) [4], and photodetectors [5]. Those optoelectronic devices integrating Si QD thin films reveal the feasibility and great potential. For example, Green *et al* first proposed integrating Si QD thin films with Si-based SCs for third generation SCs with high efficiency and low cost in 2006 [6]. The effective bandgap of Si QDs can be modified to be even greater than that of amorphous Si material (∼1.7 eV) by tuning the QD size [7]. Hong *et al* also developed Si QD thin films for SC applications and studied the doping- and size-dependent photovoltaic (PV) properties [8]. However, the results reported by Green *et al* for the all-Si QD thin film SCs in 2010 indicate that the contributions of photo-generated carriers from QDs are apparently limited because of the naturally high resistance properties of the Si-based dielectric matrix materials [9, 10]. Therefore, in order to obtain better PV properties, Si QD thin films require not only uniform QD size and heavily-doped concentration [8] but also smaller QD separation [11–13], that is, higher QD density. So far, Si QD thin films have commonly been deposited by a silicon-rich oxide single-layer (SRO-SL) or a [silicon dioxide/silicon-rich oxide] multilayer ([SiO_2/SRO]-ML) structure. The SRO-SL structure is an easy and quick deposition process for Si QD thin films, however, it is hard to control the QD size, uniformity well, and efficiently reduce the QD separation [14, 15]. Although the [SiO_2/SRO]-ML structure promises QD size control and separation reduction, a minimum thickness of 2 nm for the SiO_2 barrier layers is required to prevent the excess Si atoms in SRO layers from over-diffusing [16], which will still degrade the carrier transport efficiency [11–13]. Hence, a significantly smaller QD separation or other more suitable matrix materials [17] are indispensable for the development of SCs integrating Si QDs. In this study, we propose a new gradient Si-rich oxide multilayer (GSRO-ML) deposition structure for Si QD thin films with QD size control

 © 2013 IOP Publishing Ltd Printed in the UK & the USA

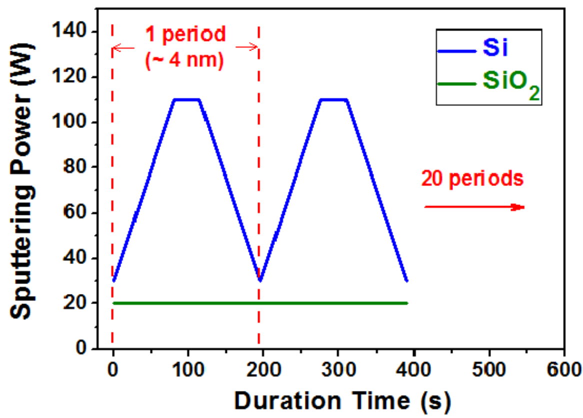

Figure 1. Variation of the Si and SiO_2 sputtering powers during deposition for sample GSRO-ML.

and separation minimization by co-sputtering deposition and high-temperature annealing methods. The nano-structural, crystalline, optical, and electro-optical properties, and the carrier transport mechanism of the Si QD thin films utilizing the GSRO-ML deposition structure are investigated and discussed.

2. Experiments

The n-type GSRO-ML thin films were deposited on p-type Si(100) wafers of 1–10 Ω cm in resistivity and fused quartz at room temperature by a radio-frequency (RF) magnetron co-sputtering deposition method. Before deposition, the Si wafers and the fused quartz were cleaned by standard RCA and ultrasonic processes individually. Si material with a phosphorus doping concentration of $\sim 1 \times 10^{18}$ cm^{-3} and pure SiO_2 material were used as the sputtering targets. The sputtering power of Si (P_{Si}) for each GSRO period was increased from 30 to 110 W at a rate of 1 W s^{-1} and held at 110 W for 1 nm thickness, then decreased from 110 to 30 W also at a rate of 1 W s^{-1} while that of SiO_2 (P_{SiO_2}) was fixed at 20 W, as shown in figure 1. Figure 2(a) shows the GSRO-ML thin film structure with 20 periods before and after annealing. Each GSRO period is composed of a highly SRO layer sandwiched between gradient SRO layers for a total thickness of 4 nm during deposition, and a super-high QD density is expected to be formed after annealing at 1100 °C for 1 h. For comparison, a [SiO_2/SRO]-ML thin film with 20 periods was also fabricated, and the film structure before and after annealing is shown in figure 2(b). The SiO_2 thin-layers with 2 nm thickness and highly SRO thin-layers with 5 nm thickness was periodically deposited. The highly SRO thin-layers were co-sputtered by 110 W of P_{Si} and 10 W of P_{SiO_2}. After deposition, a high-temperature annealing process was also performed at 1100 °C for 1 h. For electro-optical properties measurements, the annealed samples were etched by a reactive ion etching (RIE) process with CHF_3 and O_2 gases to remove the top SiO_2 layers formed during annealing. After the RIE process, the Al electrodes were deposited on the top and bottom sample surfaces with 100 nm thickness by thermal evaporator, and a square electrode array with an area of 0.8 × 0.8 mm^2 and side-to-side separation of 1 mm was used as the top electrode distribution for photo-response measurements. The Raman and photoluminescence (PL) spectra were measured using a 488 nm diode-pumped solid-state laser (Horiba LabRam HR). The cross-sectional high-resolution transmission electron microscope (TEM) images were observed by a JEOL JEM-2010F transmission electron microscope. The samples for TEM images were prepared by the conventional method, including the cutting,

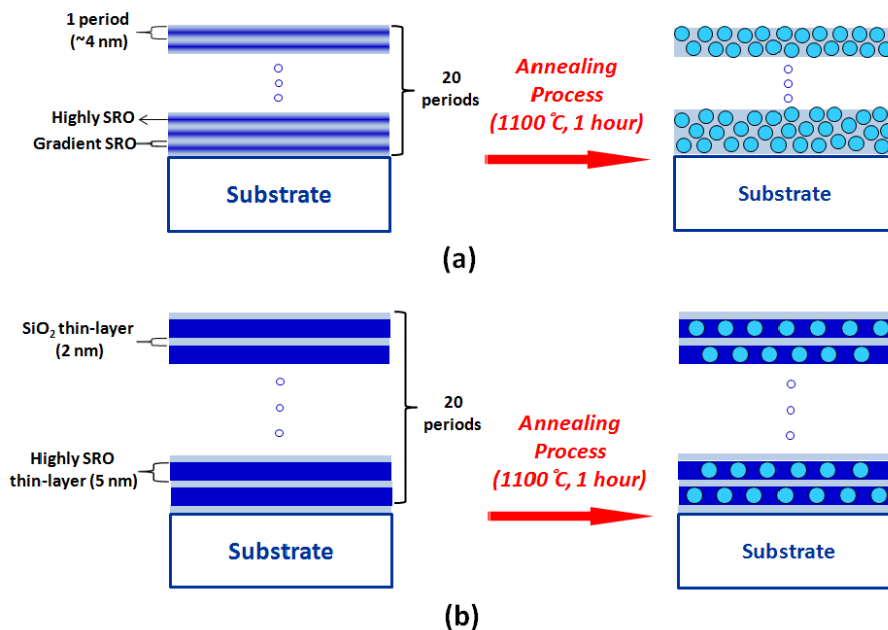

Figure 2. Illustrations of film structures for samples (a) GSRO-ML and (b) [SiO_2/SRO]-ML before and after annealing.

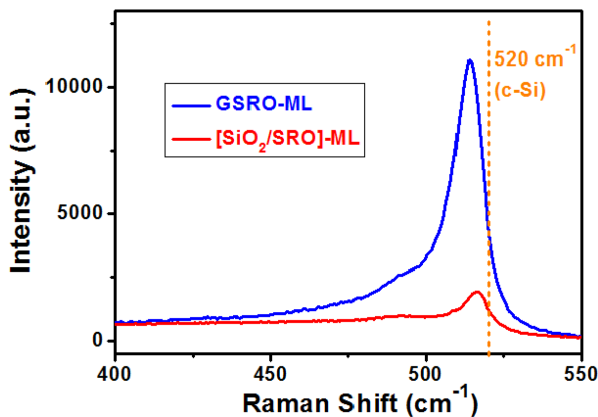

Figure 3. Raman spectra of samples GSRO-ML and $[SiO_2/SRO]$-ML.

grinding, polishing, dimpling, and ion milling processes and thinned down to electron transparency using a precision ion polishing system (Gatan 691). The absorption spectra were obtained by a UV–VIS–NIR spectrophotometer (Hitachi U-4100). The current–voltage (I–V) curves were measured using an Agilent E5270B precision measurement mainframe and a halogen lamp with a light power density of $\sim$1 mW cm^{-2} was used for photo-response measurements.

3. Results and discussions

Raman spectrum measurement is a useful, reliable, and widely-used technique for examining the nano-crystalline properties of Si materials [18, 19]. Figure 3 shows the Raman spectra of samples GSRO-ML and $[SiO_2/SRO]$-ML, in which the observed peaks near 520 cm^{-1} represent the nano-crystalline Si formation. In general, the signal can be decomposed into three components, including the peaks located at $\sim$480, 500–510, and 510–520 cm^{-1}, which originate from the transverse optical (TO) modes of Si–Si vibrations in the amorphous- (a-Si), intermediate- (i-Si), and nano-crystalline Si (nc-Si) phases [18]. The curve-fitting results from Raman spectra are listed in table 1. The similar FWHM values of the nc-Si phase for both samples indicate the close average sizes of nc-Si [19]. However, sample GSRO-ML shows not only significantly larger nc-Si intensity but also a higher Si crystal volume fraction ($f_{\text{c-Si}}$) than those of sample $[SiO_2/SRO]$-ML. This means using a GSRO-ML structure can lead to a larger amount of nc-Si with better crystal quality. Hence, compared with the commonly-used $[SiO_2/SRO]$-ML structure, our proposed GSRO-ML structure can greatly enhance the nc-Si formation while maintaining the controllability of nc-Si size for the Si QD thin films.

Figures 4(a) and (b) show the high-resolution TEM images of samples $[SiO_2/SRO]$-ML and GSRO-ML. Most of the Si QDs in sample $[SiO_2/SRO]$-ML are formed in SRO layers and separated by SiO_2 barrier layers. For sample GSRO-ML, a large number of Si QDs with closer separation is clearly observed, which indicates that a super-high density of Si QDs can be formed by using a GSRO-ML structure. Figure 4(c) shows the corresponding QD size distributions from estimating 40 QDs in samples $[SiO_2/SRO]$-ML and GSRO-ML. Both samples reveal similar QD size distributions, mainly from 4 to 6 nm, and close average QD sizes of $\sim$5.2 and $\sim$4.9 nm. However, the calculated QD density of $\sim 3 \times 10^{12}$ cm^{-2} for sample GSRO-ML is significantly higher than that of $\sim 9 \times 10^{11}$ cm^{-2} for sample $[SiO_2/SRO]$-ML, which is close to the QD density calculated from the reports by Conibeer *et al* and Zacharias *et al* [6, 16]. Therefore, the Si QD thin film using a GSRO-ML structure shows excellent capabilities not only the QD size control but also the super-high QD density formation, and such results are very helpful for SC applications integrating Si QDs.

The effective bandgap and light emission properties of the Si QD thin films have been widely investigated by PL spectrum [20–22]. The main PL emissions are from the quantum confinement (PL_{QC}) effect accompanying lower and higher energy emissions because of the carrier recombination via the interface defect states ($PL_{\text{D-interface}}$) between Si QDs and the SiO_2 matrix and the defect states in the SiO_2 matrix ($PL_{\text{D-SiO}_2}$) respectively [20–22]. Figure 5 shows the PL spectra and the fitting curves of samples GSRO-ML and $[SiO_2/SRO]$-ML, and the curve-fitting results are given in table 2. Broad PL emission properties are observed in both samples, and they can be nicely decomposed into three components, contributed by PL_{QC}, $PL_{\text{D-interface}}$, and $PL_{\text{D-SiO}_2}$. The effective bandgap obtained from the peak position of PL_{QC} in sample GSRO-ML is a little larger than that in sample $[SiO_2/SRO]$-ML, mainly owing to the slightly smaller average QD size [16], but not the closer QD separation, which will lead to an energy red shift [13]. In

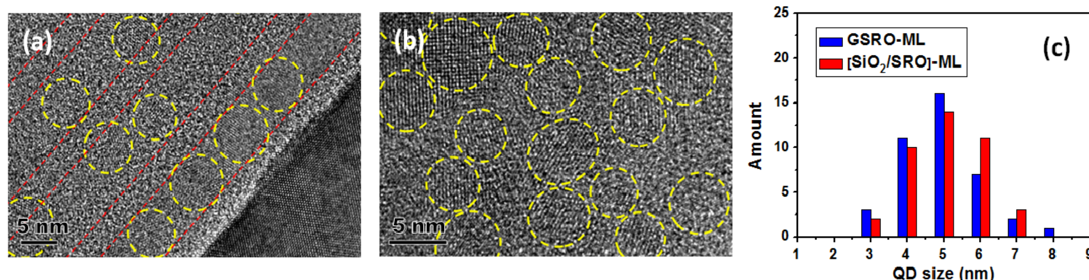

Figure 4. High-resolution TEM images of samples (a) $[SiO_2/SRO]$-ML and (b) GSRO-ML. (c) The corresponding QD size distributions.

Table 1. Curve-fitting results from Raman spectra for the Si crystalline properties of samples GSRO-ML and $[SiO_2/SRO]$-ML.

Sample	TO mode of nc-Si phase			Si crystal volume fraction ($f_{c\text{-}Si}$) (%)
	Peak position (cm^{-1})	FWHM (cm^{-1})	Integrated intensity per nanometer in thickness (au)	
GSRO-ML	514.0	9.8	1.4×10^2	73.0
$[SiO_2/SRO]$-ML	516.3	9.7	1.2×10^1	68.4

Table 2. Curve-fitting results from PL spectra of samples GSRO-ML and $[SiO_2/SRO]$-ML.

Sample	Defect states in SiO_2 matrix ($D\text{-}SiO_2$)		Quantum confinement effect (QC)		Interface defect states (D-interface)	
	Peak position	Integrated intensity (au)	Peak position	Integrated intensity (au)	Peak position	Integrated intensity (au)
GSRO-ML	2.15 eV (577 nm)	8.0×10^4	1.76 eV (705 nm)	4.6×10^4	1.52 eV (816 nm)	1.5×10^3
$[SiO_2/SRO]$-ML	2.05 eV (604 nm)	1.4×10^4	1.68 eV (740 nm)	3.7×10^5	1.46 eV (848 nm)	6.0×10^4

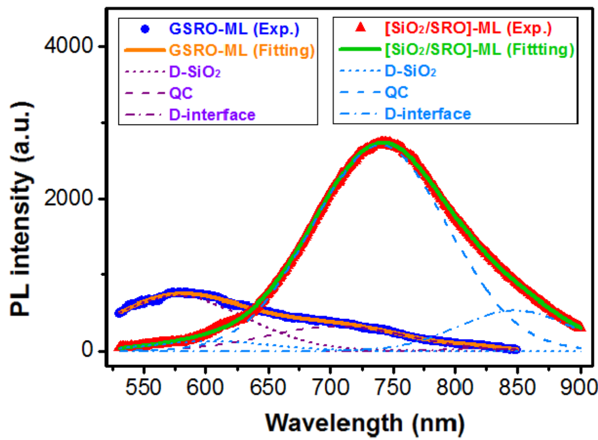

Figure 5. PL spectra and the fitting curves of samples GSRO-ML and $[SiO_2/SRO]$-ML.

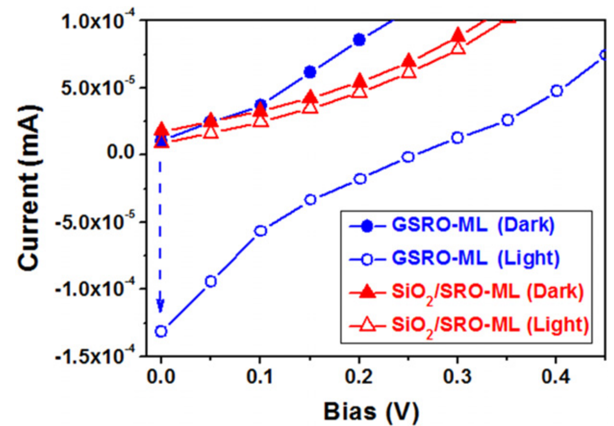

Figure 6. *I–V* curves of samples GSRO-ML and $[SiO_2/SRO]$-ML with and without 488 nm laser illumination.

addition, sample GSRO-ML, with higher QD density, exhibits a considerably lower PL_{QC} intensity than that of sample $[SiO_2/SRO]$-ML. This indicates that more photo-generated carriers can transport through QDs rather than recombine inside QDs during PL spectrum measurement since the QD separation is significantly reduced. The increased $PL_{D\text{-}SiO_2}$ in sample GSRO-ML is a reasonable result because the all Si-rich oxide matrix is used and more Si excess atoms will be left behind inside the SiO_2 matrix after Si QDs formation [22]. Since a suitable number of defect states inside the SiO_2 matrix can improve the carrier transport efficiency for the Si QD thin films [11, 12], the Si QD thin film using a GSRO-ML structure is more advantageous for SC applications. Therefore, the PL measurement results of the Si QD thin film using the proposed GSRO-ML structure with super-high QD density and good QD size control reveal better properties and the capability of effective bandgap engineering even though the Si QDs are closely formed.

To further confirm the cause of the reduced PL_{QC} emission in sample GSRO-ML, figure 6 shows the *I–V* curves of samples GSRO-ML and $[SiO_2/SRO]$-ML with and without a 488 nm laser illumination, which is used for PL spectrum measurements. A much more obvious I_{SC} enhancement is observed in sample GSRO-ML than that in sample $[SiO_2/SRO]$-ML in the light *I–V* curves. This verifies that the reduced PL_{QC} emission in sample GSRO-ML is mainly caused by the better carrier transport properties resulting from the closer QD separation than that in sample $[SiO_2/SRO]$-ML.

In order to understand the optical absorption properties of samples GSRO-ML and $[SiO_2/SRO]$-ML, the absorption spectra are measured and shown in figure 7. The absorption coefficient of sample GSRO-ML is clearly larger than that of sample $[SiO_2/SRO]$-ML owing to the higher QD density. The inset of figure 7 shows the Tauc plot for the indirect allowed transition. The optical bandgap ($E_{g,opt}$) can be evaluated by linearly extrapolating the interception at the energy axis ($\alpha h\nu = 0$) from the plot of $(\alpha h\nu)^{1/2}$ as a function of incident photon energy ($h\nu$), where α is the optical absorption coefficient [23]. The obtained $E_{g,opt}$ of samples GSRO-ML and $[SiO_2/SRO]$-ML are 1.96 and 1.83 eV, and the corresponding α values are 3.4×10^3 and 3.1×10^2 cm^{-1}. The slightly larger $E_{g,opt}$ of sample GSRO-ML than that of sample $[SiO_2/SRO]$-ML matches with

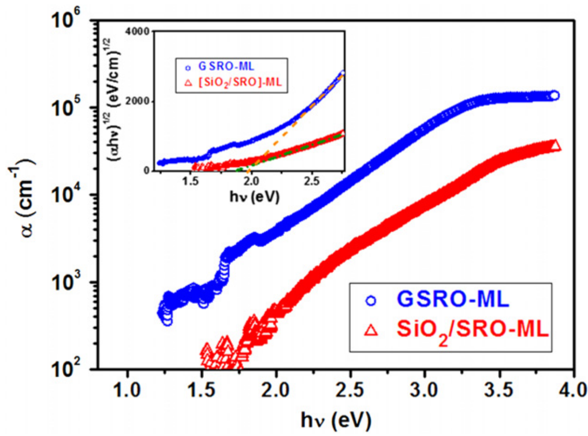

Figure 7. Absorption spectra of samples GSRO-ML and $[SiO_2/SRO]$-ML. Inset shows the corresponding Tauc plots for the indirect allowed transition.

the obtained results of effective bandgap from PL_{QC} emission, which is contributed from the small difference in average QD size. Furthermore, the α value of sample GSRO-ML is significantly improved to be over 10 times larger than that of sample $[SiO_2/SRO]$-ML and close to that of amorphous Si material [24]. This means the Si QD thin films using a GSRO-ML structure can contribute better photo-responsive properties and greatly reduce the required film thickness for SC applications. Therefore, our proposed GSRO-ML structure makes the Si QD thin film more practical and feasible for commercial SCs development.

Figure 8 shows an illustration of the device structure for I–V measurements and the dark and light I–V curves of samples GSRO-ML and $[SiO_2/SRO]$-ML. Both samples reveal rectification behavior as a diode. However, the better I–V characteristics, including a lower turn-on voltage and a higher forward current, are obtained in sample GSRO-ML. The inset of figure 8(b) shows the corresponding light I–V curves under a halogen lamp illumination with $\sim$1 mW cm^{-2} power density. The V_{OC} and I_{SC} for sample GSRO-ML are 302 mV and 5.5×10^{-4} mA, significantly larger than 110 mV and 2.6×10^{-5} mA for sample $[SiO_2/SRO]$-ML. The electro-optical properties of the Si QD thin film are efficiently enhanced by using the GSRO-ML structure.

To investigate the carrier transport mechanism, the dark forward I–V curves of samples $[SiO_2/SRO]$-ML and GSRO-ML are plotted on a log–log and shown in figure 9. For sample $[SiO_2/SRO]$-ML, the combination of the direct and phonon-assisted tunneling mechanisms is fitted with the experimental result, which is consistent with the conclusion from Osinniy *et al* [25]. For sample GSRO-ML, instead of the direct and phonon-assisted tunneling mechanisms, the two-diode mode is more appropriate to describe its forward current [26]. The current increases linearly with the bias in the low bias region (region I, $V < 0.3$ V), exponentially with the bias in the intermediate bias region (region II, $V =$ 0.3–1.5 V), and deviates from exponential behavior in the higher bias region (region III, $V > 1.5$ V). The clearly distinct conductive regions indicate a corresponding change in the dominant carrier transport mechanism. The two-diode mode had also been observed from the heavily P-doped Si QD thin films integrated with B-doped Si wafer and discussed by Park *et al* [26]. The linear relationship between log I and log V in region I indicates the presence of a parallel current path due to a shunt resistor (R_{sh}) in parallel to the junction. In region II, a feature of the current exponentially increasing with the applied voltage is dominated by the space-charge-limited current (SCLC) mechanism. In region III, the cause of the I–V characteristics deviating from the ideal behavior is still uncertain, but possibly due to the trapping states distribution. From figure 8(b), the improved PV properties observed in sample GSRO-ML represent that the SCLC mechanism is a more suitable carrier transport mechanism for SC applications integrating Si QDs owing to the largely enhanced tunneling probability or the mini-band formation resulting from the quite close distribution of Si QDs in sample GSRO-ML [11–13]. Besides, since the Si QD thin film utilizing the heavily-doped $[SiO_2/SRO]$-ML structure can possess a better carrier transport property than the normally-doped one [8], we believe it is most feasible to achieve even better PV properties by using a heavily-doped GSRO-ML structure.

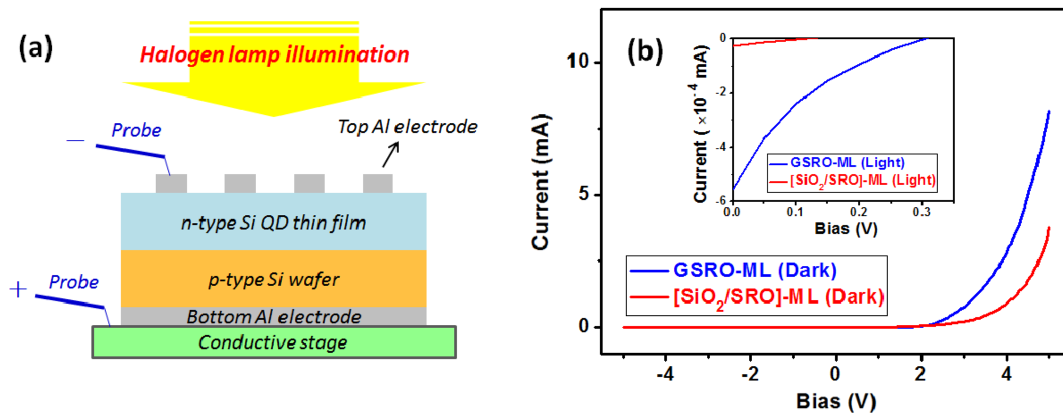

Figure 8. (a) Illustration of the device structure for I–V measurements and (b) the dark I–V curves of samples GSRO-ML and $[SiO_2/SRO]$-ML. Inset shows the corresponding light I–V curves under halogen lamp illumination.

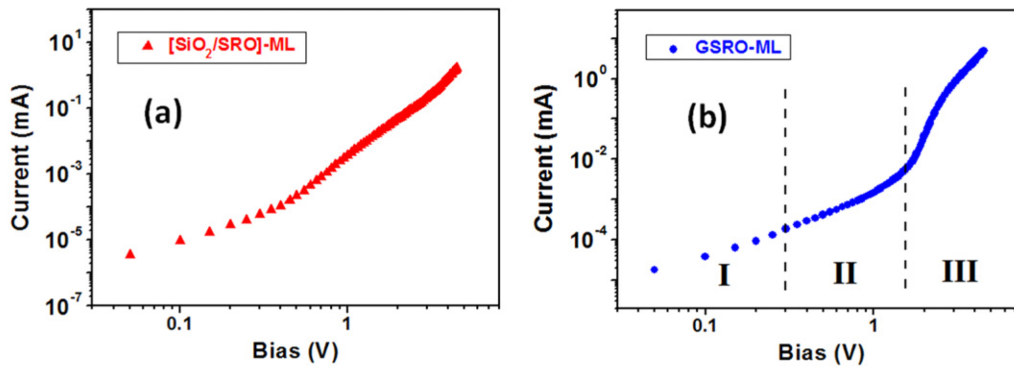

Figure 9. Dark forward *I–V* curves on a log–log scale for samples (a) $[SiO_2/SRO]$-ML and (b) GSRO-ML.

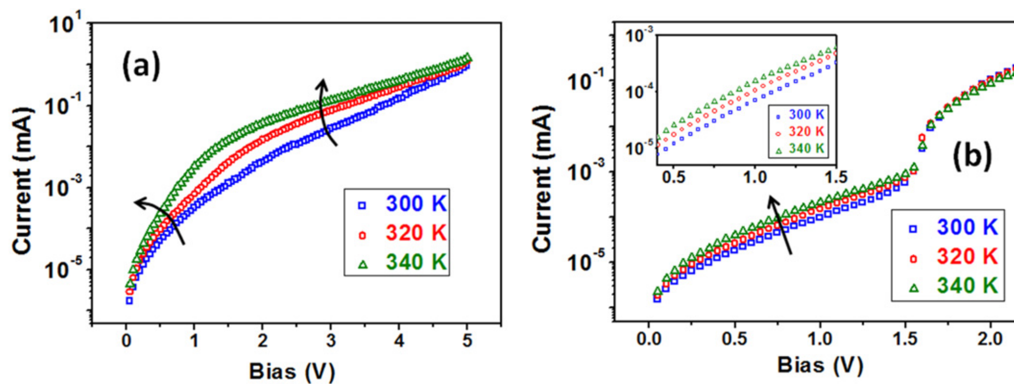

Figure 10. Temperature-dependent dark *I–V* curves of samples (a) $[SiO_2/SRO]$-ML and (b) GSRO-ML. Inset of (b) shows the magnified curves in region II.

The temperature-dependent dark *I–V* curves of samples $[SiO_2/SRO]$-ML and GSRO-ML are also examined and shown as figure 10 for further confirmation of the carrier transport mechanism. Two kinds of transport mechanism in sample $[SiO_2/SRO]$-ML are gradually discriminated by increasing temperature, as shown in figure 10(a). Such temperature-dependent *I–V* characteristics result from the direct and phonon-assisted tunneling mechanisms [25, 27]. For sample GSRO-ML, the slopes of the temperature-dependent *I–V* curves are equal in region II, as shown as the inset of figure 10(b). This indicates that the carrier transport mechanism is dominated by the SCLC mechanism [26]. The temperature-dependent ideality factors are 13–14, which are larger than 2 due to the trapping defect states or the current crowding effect usually observed in the Si nano-structured thin films [28, 29]. Therefore, from the temperature-dependent *I–V* measurements, we confirm the different carrier transport mechanisms between samples $[SiO_2/SRO]$-ML and GSRO-ML. The super-high density Si QD thin film achieved using the proposed GSRO-ML structure can truly improve the carrier transport efficiency through the SCLC mechanism.

4. Conclusion

In summary, we propose a novel deposition structure to realize Si QD thin films with enhanced PV properties. By using a GSRO-ML thin film structure, a super-high density Si QD thin film with good QD size control is demonstrated. Compared with a $[SiO_2/SRO]$-ML structure, sample GSRO-ML has improved carrier transport efficiency and a larger optical absorption coefficient resulting from the formation of QDs with significantly higher density. The over 10 times better optical absorption means the required film thickness for SC application can be greatly reduced. As a result, considerable enhancements on electro-optical properties, including the rectification, I_{SC}, and V_{OC}, are obtained. The carrier transport mechanism is also investigated. Instead of the combination of the direct and phonon-assisted tunneling mechanisms as observed in sample $[SiO_2/SRO]$-ML, the two-diode mode is found in sample GSRO-ML even though only a generally-doped concentration is used. Therefore, high efficiency Si-based solar cells integrating Si QDs can most definitely be expected using this GSRO-ML structure.

Acknowledgments

This work is supported by Taiwan's National Science Council (NSC) under contract number NSC-101-3113-P-009-004. The authors are grateful for assistance from Center for Nano Science and Technology (CNST) of National Chiao Tung University and National Nano Device Laboratories (NDL) in Taiwan.

References

[1] Wolkin M V, Jorne J, Fauchet P M, Allan G and Delerue C 1999 Electronic states and luminescence in porous silicon

quantum dots: the role of oxygen *Phys. Rev. Lett.* **82** 197–200

[2] Garoufalis C S, Zdetsis A D and Grimme S 2001 High level *ab initio* calculations of the optical gap of small silicon quantum dots *Phys. Rev. Lett.* **87** 276402

[3] Cho E C, Park S, Hao X, Song D, Conibeer G, Park S C and Green M A 2008 Silicon quantum dot/crystalline silicon solar cells *Nanotechnology* **19** 245201

[4] Cheng C H, Wu C L, Chen C C, Tsai L H, Lin T H and Lin G R 2012 Si-rich Si_xC_{1-x} light-emitting diodes with buried Si quantum dots *IEEE Photon. J.* **4** 1762–75

[5] Shieh J M, Yu W C, Huang J Y, Wang C K, Dai B T, Jhan H Y, Hsu C W, Kuo H C, Yang F L and Pan C L 2009 Near-infrared silicon quantum dots metal-oxide-semiconductor field-effect transistor photodetector *Appl. Phys. Lett.* **94** 241108

[6] Conibeer G *et al* 2006 Silicon nanostructures for third generation photovoltaic solar cells *Thin Solid Films* **511/512** 654–62

[7] Cho E C *et al* 2007 Silicon quantum dots in a dielectric matrix for all-silicon tandem solar cells *Adv. OptoElectron.* **2007** 69578

[8] Hong S H, Park J H, Shin D H, Kim C O, Choi S H and Kim K J 2010 Doping- and size-dependent photovoltaic properties of p-type Si-quantum-dot heterojunction solar cells: correlation with photoluminescence *Appl. Phys. Lett.* **97** 072108

[9] Conibeer G *et al* 2010 Silicon quantum dot based solar cells: addressing the issues of doping, voltage and current transport *Prog. Photovolt. Res. Appl.* **19** 813–24

[10] Bartzsch H, Glöß D, Frach P, Gittner M, Schultheiß E, Brode W and Hartung J 2009 Electrical insulation properties of sputter-deposited SiO_2, Si_3N_4 and Al_2O_3 films at room temperature and 400 °C *Phys. Status Solidi* a **206** 514–9

[11] Jiang C W, Green M A, Cho E C and Conibeer G 2004 Resonant tunneling through defects in an insulator: modeling and solar cell applications *J. Appl. Phys.* **96** 5006–12

[12] Green M A *et al* 2005 All-silicon tandem cells based on 'artificial' semiconductor synthesised using silicon quantum dots in a dielectric matrix *Proc. 20th European Photovoltaic Solar Energy Conf. and Exhibition (Barcelona)* pp 3–6

[13] Luo J W, Stradins P and Zunger A 2011 Matrix-embedded silicon quantum dots for photovoltaic applications: a theoretical study of critical factors *Energy Environ. Sci.* **4** 2546–57

[14] Lin C F, Tseng W T and Feng M S 2000 Formation and characteristics of silicon nanocrystals in plasma-enhanced chemical-vapor-deposited silicon-rich oxide *J. Appl. Phys.* **87** 2808–15

[15] Kim T W, Cho C H, Kim B H and Park S J 2006 Quantum confinement effect in crystalline silicon quantum dots in silicon nitride grown using SiH_4 and NH_3 *Appl. Phys. Lett.* **88** 123102

[16] Zacharias M, Heitmann J, Scholz R, Kahler U, Schmidt M and Blasing J 2002 Size-controlled highly luminescent silicon nanocrystals: a SiO/SiO_2 superlattice approach *Appl. Phys. Lett.* **80** 661–3

[17] Kuo K Y, Hsu S W, Huang P R, Chuang W L, Liu C C and Lee P T 2012 Optical properties and sub-bandgap formation of nano-crystalline Si quantum dots embedded ZnO thin film *Opt. Express* **20** 10470–5

[18] Cheng Q, Tam E, Xu S and Ostrikov K 2010 Si quantum dots embedded in an amorphous SiC matrix: nanophase control by non-equilibrium plasma hydrogenation *Nanoscale* **2** 594–600

[19] Viera G, Huet S and Boufendi L 2001 Crystal size and temperature measurements in nanostructured silicon using Raman spectroscopy *J. Appl. Phys.* **90** 4175–83

[20] Min K S, Shcheglov K V, Yang C M, Atwater H A, Brongersma M L and Polman A 1996 Defect-related versus excitonic visible light emission from ion beam synthesized Si nanocrystals in SiO_2 *Appl. Phys. Lett.* **69** 2033–5

[21] Wen X, Dao L V, Hannaford P, Cho E C, Cho Y H and Green M A 2007 Excitation dependence of photoluminescence in silicon quantum dots *New J. Phys.* **9** 337

[22] Wen X, Dao L V and Hannaford P 2007 Temperature dependence of photoluminescence in silicon quantum dots *J. Phys. D: Appl. Phys.* **40** 3573–8

[23] Meier C, Gondorf A, Lüttjohann S, Lorke A and Wiggers H 2007 Silicon nanoparticles: absorption, emission, and the nature of the electronic bandgap *J. Appl. Phys.* **101** 103112

[24] Yoshida N, Shimizu Y, Honda T, Yokoi T and Nonomura S 2008 A study of absorption coefficient spectra in a-Si:H films near the transition from amorphous to crystalline phase measured by resonant photothermal bending spectroscopy *J. Non-Cryst. Solids* **354** 2164–6

[25] Osinniy V, Lysgaard S, Kolkovsky V, Pankratov V and Larsen A N 2009 Vertical charge-carrier transport in Si nanocrystal/SiO_2 multilayer structures *Nanotechnology* **20** 195201

[26] Park S, Cho E, Song D, Conibeer G and Green M A 2009 n-type silicon quantum dots and p-type crystalline silicon heteroface solar cells *Sol. Energy Mater. Sol. Cells* **93** 684–90

[27] Wong H and Iwai H 2006 On the scaling issues and high-*k* replacement of ultrathin gate dielectrics for nanoscale MOS transistors *Microelectron. Eng.* **83** 1867–904

[28] Lau H W, Tan O K and Trigg D A 2006 Charge injection and tunneling mechanism of solid state reaction silicon nanocrystal film *Appl. Phys. Lett.* **89** 113119

[29] Perez-Wurfl I, Hao X, Gentle A, Kim D H, Conibeer G and Green M A 2009 Si nanocrystal p–i–n diodes fabricated on quartz substrates for third generation solar cell applications *Appl. Phys. Lett.* **95** 153506